

Evolutionary models for disk galaxies, a comparison with the observations up to intermediate redshifts ($z \lesssim 1$)

Claudio Firmani¹

Centro de Instrumentos-UNAM, A.P. 70-186, 04510 México D. F., México; and
 Instituto de Astronomía-UNAM, A.P. 70-264, 04510 México D. F., México

and

Vladimir Avila-Reese²

Instituto de Astronomía-UNAM, A.P. 70-264, 04510 México D. F., México

ABSTRACT

We present a scenario for the formation and evolution of disk galaxies within the framework of an inflationary cold dark matter universe, and we compare the results with observations ranking from the present-day up to $z \sim 1$. The main idea in this scenario is that galactic disks are built-up inside-out by gas infall with an accretion rate driven by the cosmological mass aggregation history (MAH). In Avila-Reese et al. (1997) the methods to generate the MAHs of spherical density fluctuations from a Gaussian random field, and to calculate the gravitational collapse and virialization of these fluctuations, were presented. Assuming detailed angular momentum conservation during the gas (5% of the total mass) contraction, a disk in centrifugal equilibrium is built-up within the forming dark matter halo. The primordial angular momentum is estimated through the Zel'dovich approximation and normalized to the spin parameter λ given by analytical and numerical studies. The disk galactic evolution is followed through a physically self-consistent approach which considers (1) the gravitational interactions among the dark halo, the stellar and gas disks, and a bulge; (2) the turbulence and energy balance of the interstellar medium; (3) the star formation process due to gas disk gravitational instabilities; and (4) the secular formation of a bulge due to the gravitational instabilities of the stellar disk.

We find that the main disk galaxy properties and their correlations are basically established by the combination of three fundamental physical factors: the mass, the MAH, and the spin parameter λ . Models calculated for a statistically significant range of values for these factors predict nearly exponential disk surface brightness profiles with realistic central surface brightnesses μ_{B_0} , and scale lengths (including low surface brightness galaxies), nearly flat rotation curves, and negative gradients in

¹Email address: firmani@astroscu.unam.mx

²Email address: avila@astroscu.unam.mx

the B-V color index radial distribution. The main trends across the Hubble sequence of the global intensive properties such as B-V, μ_{B_0} , the gas fraction f_g , and the bulge-to-disk ratio b/d, are reproduced. For a given mass (luminosity) B-V correlates with the maximum circular velocity, and this correlation is in agreement with the scatter of the Tully-Fisher relation. We interpret the observed color-magnitude, and “color ” Tully-Fisher relations as a result of the empirical dependence of extinction on luminosity (mass). The model properties tend to form a biparametrical sequence, where B-V and μ_{B_0} could be the two parameters. The star formation history depends on the MAH and on the λ parameter. A maximum in the star formation rate for most of the models is attained at $z \sim 1.5 - 2.5$, where this rate is approximately 2.5-4.0 times larger than the present one. The scale radii and the bulge-to-total ratio decrease with z , while μ_{B_0} increase. The B-band TF relation remains almost the same at different redshifts. Our scenario of disk galaxy formation and evolution reveals that the cosmological initial conditions are able to determine the main properties of disk galaxies across the Hubble sequence and predict evolutionary features for the present-day dominant galaxy population that are in agreement with very recent deep field observational studies

Subject headings: galaxies: evolution — galaxies: formation — cosmology: theory

1. Introduction

The understanding of the formation and evolution of galaxies is one of the clearest challenges of contemporary astrophysics and cosmology. Since galaxies are both cosmological and astronomical objects, two general approaches can be used in order to study their formation and evolution (e.g., Renzini 1994): (*i*) the deductive approach, through which, starting from some initial conditions given by a theory of cosmic structure formation, one tries to follow the evolutionary processes until the reconstruction of the observable properties of the galaxies and (*ii*) the inductive approach, in which, starting from the present-day properties of galaxies, and through galactic evolutionary models, one tries to reconstruct the initial conditions of galaxy formation; the increasing observational data on galaxies at intermediate and high redshifts will enrich this approach with crucial constraints.

Most of current theories about cosmic structure formation are based on the gravitational paradigm and on the inflationary cold dark matter (CDM) cosmological models. Since these models predict more power for the small density fluctuation scales than for the larger ones, cosmic structures build up hierarchically, through a continuous aggregation of mass. From the point of view of the galaxy cosmogony, a crucial question is whether this aggregation occurs through violent mergers of collapsed substructures and/or through a gentle process of mass aggregation. This question depends on the statistical distribution of the density fluctuation field and on its

power spectrum. Nevertheless, even if the dark matter structures assemble through chaotic and violent mergers of subunits, the baryon gas, because of the reheating due to the shocks implied in the collapse, virialization and star formation (SF) feedback processes, will tend to aggregate around the density peaks in a more (spatially) uniform fashion than dark matter do it. Within the framework of the hierarchical clustering theory, from the most general point of view, two could be the galaxy formation scenarios. In one case, the main properties of galaxies, including those which define their morphological types, are supposed to be basically the result of a given sequence of mergers. This picture, that we shall call the *merger scenario*, has been widely applied in semianalytical models of galaxy formation where galaxies are constructed from the cosmological initial conditions through preconceived recipes (e.g., Lacey et al. 1993; Kauffmann, White, & Guiderdoni 1993; Cole et al. 1994; Kauffmann 1995, 1996, Baugh, Cole, & Frenk 1996). In the other case, the formation and evolution of galaxies is related to a gentle and coherent process of mass aggregation dictated by the forms of the density profiles of the primordial fluctuations: galaxies continuously grow inside-out. We shall call this picture, firstly developed by Gunn (1981, 1987), and by Ryden & Gunn (1987), the *extended collapse scenario*. Since disk galaxies ($\sim 80\%$ of present-day normal galaxies) could not have suffered major mergers due to the dynamical fragility of the disks (Tóth & Ostriker 1992), the extended collapse scenario results more appropriate to study their evolution.

According to the merger scenario, the bulges of spiral galaxies and the elliptical galaxies arise from the mergers of galactic disks. A natural prediction of this scenario is that spirals with small bulge-to-disk ratios should have bulges older than those of spirals with large bulge-to-disk ratios (e.g., Kauffmann 1996). As Wyse, Gilmore, & Franx (1997) have pointed out this does not appear compatible with recent observational data (de Jong 1996a; Peletier & Balcells 1996; Courteau, de Jong, & Broeils 1997). On the other hand, if elliptical galaxies are the product of relatively recent mergers, then a big dispersion is expected in their color-magnitude relationship (but see Kauffmann 1996). Bower, Lucey, & Ellis (1992) showed that for the ellipticals in the Coma Cluster, this relationship is extremely tight. Ellis et al. (1997) confirmed this result for ellipticals in intermediate redshift clusters, up to $z \sim 0.6$. The merger scenario could also have serious difficulties from the dynamical point of view: it is not conclusive if mergers of disks are able to reproduce the high central phase-space densities of elliptical galaxies (e.g. Hernquist 1993).

The inductive approach yields the possibility to establish several constraints to the galaxy formation and evolution processes. Galactic evolutionary models have shown that due to the rapid disk gas consumption in SF, closed models are not able to explain several properties of disk galaxies, as well as the wide range of colors, gas fractions, etc. that galaxies present across the Hubble sequence (e.g., Larson & Tinsley 1978; Tinsley 1980; Larson, Tinsley, & Caldwell 1980; Kennicutt 1983; Gallagher, Hunter, & Tutukov 1984; Firmani & Tutukov 1992, 1994). On the other hand it was shown that the SF time scale in disk galaxies is not controlled by the initial gas surface density (Kennicutt 1983; Kennicutt, Tamblyn, & Congdon 1994). Hence, models where gas accretion is introduced are more realistic. Gas accretion could also be necessary to maintain

spiral structure. In the case of open models, galaxy formation and galactic evolution might be two related processes where the SF time scale is driven by the gas accretion rate at which the disk is being built up. Infall models of disk galaxy formation have been recently favored by studies of our own Galaxy and nearby galaxies (see for references Cayón, Silk, & Charlot 1996). Moreover these inside-out disk formation models seem also to be in agreement with constrictions provided by deep field observations (e.g., Bouwens, Cayón, & Silk 1997; Cayon et al. 1996; see also Section 4).

The gas infall rate in luminous galaxies may be controlled by the global process of galaxy formation (cosmological accretion) and/or by a self-regulated process of SF formation. This latter process proposed by White & Rees (1978) and White & Frenk (1991) is commonly applied in the merger scenario models. According to this mechanism, the gas accretion rate is driven by the cooling of the hot gas corona sustained by the supernova-injected energy. In the extreme situation of instantaneous galaxy formation, supernova gas reheating, halo self-regulated SF, and cooling flows (if the reheated gas was not completely expelled out of the system) become the dominant processes in regulating luminous galaxy evolution. However, the self-regulated halo SF model suffers from some inconsistencies. As Nuslen & Fabian (1996) pointed out, supernova feedback over large scales occurs on roughly the same time scales as the SF, not fast enough to tightly regulate the SF rate. In the same way, if a disk forms, then the self-regulating mechanism of SF will apply to the disk where other dynamical conditions prevail (see Firmani, Hernández, & Gallagher 1996), and not to the halo system. Unless the disk-halo connection is very effective, the SF in the disk will not be regulated by a balance of energy between the supernova input and the halo gas cooling. On the other hand, the X-ray gas corona predicted by the self-regulated SF mechanism lacks observational support, at least for the most massive galaxies for which the X-ray emission would have been above the minimum detection limits of the Rosat and ASCA experiments.

The galactic infall models suggested by the inductive approach, are consistent with the cosmological (deductive) extended collapse scenario of galaxy formation and evolution. In Avila-Reese, Firmani, & Hernández (1997, hereafter AFH), within the framework of a standard CDM model, the MAHs corresponding to fluctuations of galactic scales were generated from the statistical properties of a Gaussian random field. After calculating the virialization of the fluctuations, a range of realistic dark halo structures were obtained. Now, with the aim to explore whether these cosmological initial conditions are able to predict the evolutionary and observational disk galaxy properties and their correlations, particularly those which go across the Hubble sequence (HS), we shall construct a self-consistent and unified model of disk galaxy formation and evolution in the cosmological context. Within the framework of the extended collapse scenario and using the galactic evolutionary models of Firmani et al. (1996), we shall study the formation and evolution of disks in centrifugal equilibrium into the evolving dark halos. In section 2, the methods we use are described. The model results at $z = 0$, the main predictions of the models, and the comparisons with observations as regards the local (§3.1) and global galactic properties and their main correlations (§3.2) are presented in section 3. In section 4 we compare our evolutionary

models with observations at intermediate redshifts ($z \lesssim 1$). Finally, the concluding remarks are given in section 5.

2. The Method

The first part of our approach is to calculate the gravitational collapse and virialization of isolated dark galactic halos starting from a primordial density fluctuation field. This was done in AFH and the reader is referred there for details (see also Avila-Reese 1998). We have assumed a Gaussian (random-phase) fluctuation field, for which all the statistical properties depend only on the power spectrum of fluctuations provided by the assumed cosmological model. The conditional probability for Gaussian random fields is used to calculate the mass distribution of halos at time t_{i+1} that go on to form halos of mass M_i at a later time t_i . Fixing M_0 and its cumulative density contrast at the present epoch t_0 , this distribution is recurrently applied through a Monte Carlo method to construct the MAHs of main progenitors. The MAHs were constrained to simulate isolated objects. Assuming spherical symmetry, a generalized secondary infall method was used to calculate the sequential collapse of concentric shells given by the MAH, and their “relaxation” into a stationary virialized structure. The structures obtained through our method for the standard CDM (SCDM) model are in agreement with the results of high-resolution cosmological N-body simulations. It was also shown that, for a given mass the statistical dispersion in the MAHs actually produces a sequence of different DM virialized configurations.

2.1. Disk build-up

Gas is able to cool and further collapse within the DM halo. The collapse can be halted only by centrifugal forces and/or when gas is transformed into stars. While the second case could be related to the origin of large bulges and elliptical galaxies, the former is commonly invoked to explain the formation of disk galaxies. The build-up of disks within the evolving DM halos is carried out as follows: (1) we consider that, at the beginning, baryon matter has mass and angular momentum distributions similar to those of the DM; it is assumed that the spherical shells are in solid body rotation; (2) once the current mass shell has attained its maximum expansion radius, a fraction f of its mass (gas) is transferred in a dynamical time to a disk in centrifugal equilibrium with a surface mass distribution calculated under the assumption of detailed angular momentum conservation; for galaxies the gas cooling time is typically smaller than the dynamical time (Silk 1977; Rees & Ostriker 1977; White & Rees 1978; Ryden & Gunn 1987); (3) the gravitational drag on the total system produced by the central disk is calculated at each time with the adiabatic invariant formalism (Flores et al. 1993; AFH).

The specific angular momentum j acquired by each collapsing shell during the linear regime is estimated using the Zel’dovich approximation (e.g., White 1994):

$$j \propto t_m^{1/3} M^{2/3} \propto (GM r_m)^{1/2} \quad (1)$$

where t_m is the time at the maximum expansion, M the mass inside the shell, and r_m the shell radius at the maximum expansion. The constant in (1) is given by the amplitude of the tidal torque induced by neighboring objects; obviously our approach is not able to predict it. We use the predictions of analytical studies and the outcomes of cosmological N-body simulations which are commonly expressed through the spin parameter $\lambda \equiv \frac{J|E|^{1/2}}{GM^{5/2}}$, where J and E are the angular momentum and total energy of the virialized system (e.g., Catelan & Theuns 1996 and references therein). These studies find that the distribution of λ 's is well approximated by a log normal distribution with an average value of ~ 0.05 and a width in the log less than one. It was found that the dependence of this distribution on the mass and power spectrum is weak. Therefore, we will not consider it further. We fix the constant needed in relation (1) in such a way that the λ of the virializing DM halo at every time is equal to the value we chose from the distribution mentioned above.

2.2. Disk galactic evolution

The disks which are continuously forming into the dark halos transform their gas into stars. In Firmani et al. (1996), a self-consistent approach to study the SF in its stationary regime, and the physics of the gas and star disks was presented. In this approach gas disk height and SF are regulated by an energy balance between supernova input and turbulent energy gas dissipation. Here we add the kinetic energy input due to gas accretion. Star formation runs when the Toomre gravitational instability parameter for the disk gas ($Q_g \equiv \frac{v_g \kappa}{\pi G \Sigma_g}$, κ is the epicyclic frequency, v_g the gas velocity dispersion, and Σ_g the gas surface density) is below a given threshold, *i.e.* the SF is controlled by a feedback mechanism such that, when the disk is overheated by the SF activity, SF is inhibited and the disk immediately dissipates the excess energy to lower v_g back to the value determined from the Toomre criterion. In his original study Toomre (1964) estimated for an infinitely thin disk a value of 1 for the threshold. Numerical simulations (Sellwood & Carlberg 1984; Carlberg 1985; Gunn 1987), and observational estimates (e.g., Skillman 1987; Kennicutt 1989) suggest thresholds of the order of 2; this result is attributed to collective phenomena such as the swing and “waser” amplifications which are difficult to account for in the analytical studies. In our models the value of this threshold controls the thicknesses of the gas and stellar disks; when a value of 2 is used we obtain for a model of the Galaxy gas and stellar thicknesses compatible with observations. The gas loss from stars is also included. The gravitational dynamics of the evolving disk, the DM halo, and the bulge (see below) are treated in detail. The local disk galactic models presented in Firmani & Tutukov (1994) included an integration over the evolutionary tracks of all stars formed (a Salpeter initial mass function with a minimal star mass of $0.1M_\odot$, and solar metallicities were used), allowing the calculation of luminosities in different colors. Using the results from these models the surface B-brightness and B-V color indexes may be found at every

radius and throughout the evolution of our galactic disk models (see Firmani et al. 1996). We have compared the color indexes obtained by Firmani & Tutukov (1994) with those predicted by the population synthesis of Fritze-v.Alvensleben & Gerhard (1994) for three SF histories that they identify as corresponding to Sa, Sb, and Sd galaxy types. The agreement is satisfactory. We find that the approximation to the population synthesis we use provides a B-V which is ~ 0.1 mag in the red, and ~ 0.05 mag in the blue less than the respective values given by more sophisticated models (e.g., Bruzual & Charlot 1993; Charlot, Worthey, & Bressan 1996).

2.3. Bulge formation

Recent observational and theoretical studies are changing some common preconceptions about galactic bulges; for a recent review see Wyse et al. (1997). These studies tend to show that several bulge formation mechanisms could be working in galaxies. Bulges in galaxies with low and intermediate bulge-to-disk (b/d) ratios may be formed through secular dynamical evolution of the disks, whereas bulges in galaxies with large b/d ratios could have been formed separately from the disks, through an early dissipative collapse and/or from mergers.

We have introduced a recipe to estimate the bulge mass. The stars of the central “cold” disk region where the stellar Toomre instability parameter $Q_s \equiv \frac{v_s \kappa}{3.36 G \Sigma_s}$ is less than 1, are transferred to a spherical component in such a way that Q_s remains equal to 1. The physical sense of this recipe is in agreement with the secular scenario of bulge formation where gravitational instabilities in the stellar disks produces bars which dissolve forming a “hot” component, the bulge (see Norman, Sellwood, & Hasan 1996, and references therein). Indeed, the similarity found in colors (Peletier & Balcells 1996), and scalelengths (de Jong 1996a; Courteau et al. 1997) between disk and bulge might mean that these parameters are closely associated. It is worth emphasizing that our recipe of bulge formation is a very crude approximation to a complex phenomena about which, in fact, not much is known, both from the theoretical and observational point of views.

3. The models at $z=0$

With the methods and schemes described in the previous section it is possible, from the cosmological initial conditions, to calculate the properties of disk galaxies at every time, particularly at the present-day, $z = 0$. Here our purpose is to obtain (i) the main structural and luminosity characteristics of galaxies corresponding to a local disk galaxy population, and (ii) its main correlations between global properties, particularly those which go across the HS. Once the cosmological model and the present-day mass of the object under study is given, the MAHs and their statistical distribution can be calculated through Monte Carlo simulations. To form disks in centrifugal equilibrium it is necessary to fix the spin parameter λ , and the fraction of total mass f which is incorporated in the disk. As in AFH, here we shall assume that galaxies

incorporate to the disk all the available baryons in the form of gas, and with a settled mass fraction equal to the primordial Big Bang nucleosynthesis predictions, $f_B \approx 0.05\Omega_o h_{0.5}^2$, where $h_{0.5}$ is the Hubble parameter in units of $50 \text{ kms}^{-1}\text{Mpc}^{-1}$. This assumption may not be realistic particularly for low mass (velocity) systems which lose much of gas after the first bursts of SF, giving rise to the family of dwarf galaxies (Dekel & Silk 1986). To achieve the first purpose, it is enough to calculate models for a significative range of masses, MAHs and λ 's, and test if the obtained galaxy properties for these ranges are realistic. As a first order approximation, we shall calculate models only for the average cases of the distributions of the MAHs and λ 's, and for two statistically significant deviations from the averages. Therefore, regarding the second purpose, only general trends in the correlations among the global galaxy properties will be obtained. As a matter of fact, the available observational galaxy samples are not complete enough as to provide certain statistical information on galaxy properties and their correlations. We consider three representative masses (dark+baryon matter) for normal galaxies: $5 \times 10^{10} M_\odot$, $5 \times 10^{11} M_\odot$, and $5 \times 10^{12} M_\odot$. For each mass three MAHs are selected, the average, and two symmetrical deviations in such a way that roughly 80% of all the MAHs are contained between them (see AFH). For each mass, and for each MAH, we shall calculate models taking three values for λ : 0.035, 0.05, and 0.1. As in AFH, with the aim of studying general behavior, only one representative cosmological model will be used, namely the Gaussian SCDM model normalized to $\sigma_8 = 0.57$. In AFH it was shown that the $\sigma_8 = 1$ SCDM model produces the correct slope of the I- and H-band Tully-Fisher (TF) relations, but the zero-point is too small. This disagreement with observations disappears when $\sigma_8 = 0.57$ is used, a value suggested by studies of masses and abundances of rich clusters of galaxies (White, Efstathiou, & Frenk 1993). It is worth remarking that at galactic scales the power spectrum of the flat, *COBE*-normalized $\Omega_\Lambda = 0.7$, $h = 0.65$, CDM model is very similar to that of the $\sigma_8 = 0.57$ SCDM model.

3.1. Local properties of the disk galaxy models.

In Figure 1(a) the surface B-brightness profiles of a $5 \times 10^{11} M_\odot$ model are plotted. The solid, dashed, and point-dashed lines correspond to cases with $\lambda = 0.05$, $\lambda = 0.035$, and $\lambda = 0.100$, respectively, where the thick lines are for the average MAH, and the thin lines are for the early active MAH (only the $\lambda = 0.035$ case is plotted) and the very extended MAH (only the $\lambda = 0.100$ case is plotted). It is seen that the brightness profiles are nearly exponential. For other masses the situation is the same. Although the scale radii and the central surface brightnesses fall within the corresponding ranges allowed by observations, we note that the radii and surface brightnesses of the modeled disks tend to the upper and lower limits of these ranges, respectively. If transfer of angular momentum from baryon matter to DM is considered, then the disk scale lengths decrease giving smaller and more concentrated disks. The radii and surface brightnesses of models with $\lambda = 0.1$ compare well with those of low surface brightness (LSB) galaxies. The models predict negative radial gradients in colors, as is seen in Figure 1(b) where the radial B-V distributions are shown for the same models of Figure 1(a). Accurate multiwavelength surface photometry studies

of galaxies (e.g., de Jong 1995) confirm that galactic disks tend to be bluer at the periphery, although these gradients are typically smaller than those predicted by our models. Experiments where only a moderated angular momentum redistribution in the infalling gas was introduced, show that the color gradients decrease.

In Figure 2 the rotation curves for the same models of Figure 1 are depicted. The radii were scaled to the Holmberg radii. The shape of the rotation curve depends mainly on the spin parameter λ and correlates strongly with the central surface brightness. For $\lambda=0.035$ the disk is very concentrated and the rotation curves are decreasing at the optical radii. The rotation curves corresponding to models with $\lambda = 0.05$ are nearly flat at the Holmberg radius for all the MAHs. For $\lambda = 0.1$ the rotation curves grow slowly and the disks are less concentrated than in the cases of smaller λ 's. In Figure 2, the rotation curves of the $5 \times 10^{10} M_{\odot}$ and $5 \times 10^{12} M_{\odot}$ models corresponding to the average MAHs and λ are also depicted. At the Holmberg radius the less massive models have nearly flat rotation curves, while the more massive galaxies present decreasing rotation curves. The synthetic rotation curves derived from observations (normal galaxies) in Persic, Salucci, & Stel (1996) show a similar trend, although in this case the less luminous galaxies present increasing rotation curves at the optical (\sim Holmberg) radius.

In AFH it was shown that the dark halo component typically dominates down to near the center (see Fig. 4 of AFH) in the rotation curve decomposition. This possible disagreement of the models with observations is related to the cuspy inner structure of dark matter halos. Collective dissipative mechanisms and/or the cosmological initial conditions could produce shallow cores in the dark halos (AFH). Here, we shall artificially introduce constant density cores according to the observed inner structure of dwarf and LSB galaxies. Burkert (1995) found a density profile with two parameters which fits very well the structure of dwarf galaxies: $\rho(r) = \frac{\rho_c r_c^3}{(r+r_c)(r_c^2+r^2)}$. Actually, observations show that the two parameters are correlated. Using the measured rotation curves of the same five dwarf galaxies considered in AFH, we find that $\rho_c = 0.065 \left(\frac{r_c}{\text{kpc}}\right)^{-6/7} \frac{M_{\odot}}{\text{pc}^3}$. The integration of this density profile until the present-day halo virialization radius should be equal to the given total halo mass M_0 . The spherical top-hat collapse model and energy conservation allow a rough estimate of this radius as a function of the mass: $r_h \simeq 56 \left(\frac{M_0}{10^{10} M_{\odot}}\right)^{1/3} h_{0.5}^{-2/3}$ kpc. Thus, using the $\rho_c - r_c$ dependence, it is possible to estimate r_c as a function of M_0 : $r_c \simeq 2.1 \left(\frac{M_0}{10^{10} M_{\odot}}\right)^{1/2} h_{0.5}^{-2/3}$ kpc. The Burkert density profile also fits well the structure of LSB galaxies, although the dispersion in the $\rho_c - r_c$ dependence is high. Given that the observational information is very limited we shall use the presented mass-core radius relationship only as representative of the average case. As is seen in Figure 3 the rotation curve decomposition of a $5 \times 10^{11} M_{\odot}$ model with the average MAH, and $\lambda = 0.035$, which formed in a DM halo with a core, is similar to the decompositions derived from the usual fitting techniques to observations (e.g., Carignan & Freeman 1985; van Albada et al. 1985; Begeman 1987). Even galaxies with $\lambda = 0.035$ now present a nearly flat rotation curve. This allows us to shift the λ 's to smaller values, within the uncertainty prediction range, and in this way surface densities larger than in the coreless case will be obtained. Furthermore, better agreement with the synthetic rotation curves of Persic et al.

1996 is found. In conclusion, the existence of cores in the DM halos produced in a SCDM model, directly influences the dynamical and structural properties of present-day disk galaxies, and in the correct direction.

3.2. Global properties of disk galaxies and their correlations

Among the global properties that our models predict for a disk galaxy we shall consider the integral B-V color index (calculated within a Holmberg radius), the B-band luminosity L_B , the B-band exponential disk scale length h_d , the B-band central surface brightness μ_{B_o} or Σ_{B_o} (μ_{B_o} is given in magnitudes per arcsec², and Σ_{B_o} in L_{B_\odot} per pc⁻²), the disk gas fraction f_g ($\equiv \frac{M_{gas}}{M_{gas}+M_{stars}}$), the stellar bulge-to-disk ratio b/d, and the maximum rotation velocity V_{max} . The correlation matrix from a principal component analysis of these properties for the 27 models calculated here is given in Table 1. It is seen that for the intensive properties, the observational trends across the HS are reproduced: the redder and more concentrated the disk, the smaller is the gas fraction, and the larger is b/d. Furthermore, the models seem to populate a planar region in the $\mu_{B_o} - (B - V) - f_g$ and $\mu_{B_o} - (B - V) - b/d$ spaces, in rough agreement with observations (McGaugh & de Blok 1997, hereafter M-GB). B-V and μ_{B_o} are almost independent one to another, so that we can express f_g and b/d as functions of these two parameters. In figure 4, f_g is plotted versus B-V and μ_{B_o} . The gas fraction is larger for smaller B-V (panel (a)) which means that f_g is larger for the MAHs whose present-day gas infall rate is still high. On the other hand, in panel (b) it is seen how a less concentrated disk (larger λ) presents a higher gas fraction than a disk with high Σ_{B_o} . On the basis of this result is the influence of the disk gravitational compression on the capability of gas to form stars (Firmani & Tutukov 1992, 1994). The disk surface density also strongly influences the b/d ratio because the stellar surface density enters in the Toomre gravitational instability criterion which is used in our models to calculate the formation of bulges. The larger the central surface brightness (stellar density), the larger is the b/d ratio (Figure 5 (b)). The mass and MAH introduce a dispersion in this correlation because they influence the other quantities which appear in Toomre criterion. In Figure 5(a) it is seen how marginally b/d depends on B-V. The observational data tend to confirm that b/d is more correlated to μ_{B_o} than to B-V (e.g., de Jong 1996a).

In Figures 4 and 5 are also plotted the observational data taken from a compilation presented in M-GB where LSB galaxies are included (only in Figure 4). The B-V color indexes were not corrected for the internal (inclination) galaxy extinction. We have applied this correction according to the formula given in the RC3 catalog (de Vaucouleurs et al. 1991). The b/d ratios for the LSB galaxies presented in M-GB were not estimated, so that in the panels where this ratio is plotted the LSB galaxies are not considered. In general, the models fall rather well within the observational ranges, and are in agreement with the observable correlations (compare also Table 1 with the correlation matrix presented in M-GB). It is surprising that the b/d ratios predicted by the models using the simple gravitational instability criterion are in agreement with those inferred

from observations (de Jong 1996a,b). Note that de Jong (1996b) used an exponential profile in his two dimensional bulge-to-disk decomposition procedure, instead of the de Vaucouleur’s profile for the bulges, arguing that such a profile fits the observations better. That is why the b/d ratios obtained by him are smaller than those given by previous b/d decompositions (e.g., Simien & de Vaucouleurs 1986).

Perhaps the most serious inconsistency when comparing theory with observation is that the considered models in Figures 4 and 5 do not seem to be able to attain enough red color indexes. The statistical range ($\sim 80\%$) of the MAHs calculated here for the Gaussian fluctuations leads to disks with B-V between ~ 0.4 and ~ 0.7 . We have found that the color index becomes very sensitive to the MAH when this corresponds to early high aggregation rates: for some extreme cases the B-V color may be as red as ~ 0.95 mag. Thus, some models can easily attain colors redder than 0.7; of course the frequency of such models will be low. In Figures 4 and 5, with dashed lines we show the range in the different properties of the $5 \times 10^{11} M_{\odot}$ models for the three λ 's, when the statistical range in the MAHs is symmetrically extended to 94% (symbols consider only 80%). In the case of the color index it is seen that the red extreme is very sensitive to the MAH. The Figures show that roughly 3% of models ($5 \times 10^{11} M_{\odot}$) can be redder than 0.8 mag. The very incomplete observational sample we are using here shows that $\sim 10\%$ of galaxies are redder than this magnitude. A cross sample of 330 galaxies from the RC3 (de Vaucouleurs 1991), and the Tully (1988) catalogs (see Firmani & Tutukov 1994) would give $\sim 5\%$. However, our aim in this discussion is not to claim statistical predictions, for which there would not be complete observational counterparts, but simply to point out that our models can be as red as some observed galaxies are. On the other hand, several questions not directly related to the scenario presented here might be involved in the color index problem. (1) The internal extinction in combination with the metallicity-luminosity relation can introduce an important effect of reddening, particularly for the most massive galaxies (see §3.2). Using the results presented in Wang & Heckman (1996), and the Galactic extinction curve for $R_V = 3.1$ (Cardelli, Clayton, & Mathis 1989) we have reddened the models corresponding to the average MAH and $\lambda = 0.05$, represented in Figures 4 and 5 with black filled circles. The error bars account for the range of parameter values given in Wang & Heckman (see §3.2). (2) The influence of environment on the galaxy evolution might help to produce models redder than 0.7 mag. In the dense environments the gentle mass aggregation can be early truncated and followed by a merging process between neighboring systems. Experiments show that if gas accretion is truncated in the models at 6 Gyrs (4 Gyrs) then B-V roughly increases by 0.08 (0.15) mag. On the other hand, the interactions in the dense environments can induce non stationary SF which produces a fast gas consumption in stars. (3) Although the statistical approach used to generate the MAHs has proved to be a good approximation with respect to results of cosmological N-body simulations for the average case (AFH), in the more extreme situations of highly decreasing aggregation regimes the approach is not necessarily realistic. In this approach, basically due to the Gaussian statistics (where negative densities are possible), the mass aggregation never stops. Hence, the possibility that the galaxy neighborhood is matter exhausted is never taken into account, and as was mentioned above B-V

becomes very sensitive to the MAH in the cases of highly decreasing aggregation regimes.

Although the observational sample presented in Figures 4 and 5 is statistically incomplete, it seems that observations show larger scatters in the correlations among the intensive properties than do the models. While part of the scatter is produced by the observational uncertainties and possible effects of the extinction, it is highly probable that the intrinsic scatter is in any case larger than the one predicted by the models, because the scenario proposed here does not take into account several phenomena which are not dominant, but are present in real galaxies. For example the SF prescription used in the models is basically a stationary process, while in real galaxies SF may appear in bursting modes. This fact introduces a stochastic component in the photometric features, particularly in low mass galaxies (Firmani & Tutukov 1994).

With respect to the observations, the predicted central surface brightnesses are smaller, while the gas fractions are slightly larger. It is worth emphasizing that the scenario presented here assumes detailed angular momentum conservation in the gas collapse, and all the matter accreted by the disk is considered to be only in form of gas. If some angular momentum transference from baryon matter to dark matter is present during the gas collapse, and if some (small) fraction of matter is incorporated to the galaxy in form of stellar systems (mergers), then the modeled disks would be more concentrated and less gaseous than those presented here.

The intensive properties and correlations of the models calculated with an artificial core in the DM halo do not significantly differ from models without a core. That is why we will not repeat Figures 4 and 5 for the models with a core. The most important change is related to the shape of the rotation curves: in order to obtain flat rotation curves for the average MAHs, λ should be shifted to smaller values than in the corresponding cases of coreless halos (see Figure 3), producing disks with slightly larger central surface brightnesses.

Concerning the extensive properties, the models predict close relations between mass (luminosity) and maximum rotation velocity (the Tully-Fisher (TF) relation), as well as between mass (luminosity) and scale or Holmberg radius. In AFH it was shown that the disk mass vs. maximum rotation velocity relation for the $\sigma_8 = 0.57$ SCDM model is in excellent agreement with the same relation estimated from the observed H- and I-band TF relations using the appropriate mass-to-luminosity ratios. It is interesting to note that the scatter in the mass-velocity relation (and therefore probably in the H- or I-band TF relations) is correlated with some intensive properties which define the HS. For example, in Figure 6 it is shown how, for a given mass, the maximum circular velocity increases with B-V. This dependence can be easily understood from the point of view of the extended collapse scenario: galaxies formed through gentle MAHs will be less concentrated (smaller circular velocities) and with SF histories more extended in time (bluer colors) than galaxies formed through early active MAHs. The observational data confirm this prediction of the models. In Figure 6, some galaxies from a cross of the RC3 and Tully catalogs (see above) are also depicted. To estimate the behavior of the rotation velocity with B-V for a given mass, the data were divided in 3 bins according to the B luminosities presented in the

mentioned catalogs. The dashed lines are lineal regression to each one these bins. The trend is roughly the same as in the case of the models.

The mass-radius relation predicted by the models where the average values in the MAH and λ were used is:

$$M_s \propto R_H^{2.3} \quad (2)$$

where M_s is the disk stellar mass, and R_H is the Holmberg radius. The radius scales with the B-band luminosity L_B as $R_H^{2.4}$. The Holmberg and scale radii do not correlate with any intensive galaxy property (see Table 1), suggesting that the evolution of disk galaxies and the HS are size independent (de Jong 1996a; M-GB).

The models do not predict any correlation between B-magnitude (or stellar disk mass) and color, and the average B-band TF relation we obtain is $\frac{L_B}{L_{B\odot}} = 200 \left(\frac{V_{\max}}{\text{km s}^{-1}} \right)^{3.5}$. Observational data point to a correlation between magnitudes and colors (e.g., Vishnavatan 1981; Wyse 1982; Tully, Mould, & Aaranson 1982; Gavazzi 1993; Wang & Heckman 1996), and show slopes in the B-band TF relation smaller than in the cases of the TF relations at longer wavelengths (for a review see Strauss & Willick 1995); these points are related to one another. By dividing the B-band TF relation $L_B = A_B V_{\max}^{m_B}$ by, for instance, the H-band TF relation $L_H = A_H V_{\max}^{m_H}$, one obtains:

$$(B - H) = 2.5 \left(\frac{m_H}{m_B} - 1 \right) \log L_B + 2.5 \log \left(\frac{A_H}{A_B^{m_H/m_B}} \frac{L_{B\odot}}{L_{H\odot}} \right) \quad (3)$$

For the values of m_B and m_H reported in the literature eq. (3) gives $(B-H) \propto \alpha \log L_B$ with $\alpha \approx 0.4 - 1.2$ in rough agreement with the reported magnitude-color relations. Within the framework of the galactic evolutionary models presented here, the *SF history is not able* to account for this dependence. It is possible that the observed luminosity-metallicity relation and dust extinction in galaxies are responsible for this dependence. In the last few years the number of studies which point out to non-negligible face-on extinction corrections have increased (see references in Wang & Heckman 1996, and Boselli & Gavazzi 1994). Wang & Heckman (1996), based on studies of the far UV and FIR fluxes of a sample of normal late type galaxies, have concluded that the dust opacity increases with the luminosity of the young stellar population. Through models of absorption and emission of radiation by dust in uniform plane-parallel slabs they find that a power law optical depth vs. UV luminosity relation explains this observational dependence. This relation referred to the B band is:

$$\tau_B = \tau_{B,*} \left(\frac{L_B}{L_{B,*}} \right)^\beta \quad (4)$$

where the best fits to observations are for $L_{B,*} = 1.3 \times 10^{10} L_{B\odot}$, $\tau_{B,*} = 0.8 \pm 0.3$, and $\beta = 0.5 \pm 0.2$. According to the uniform slab model, the extinction in magnitudes may be

expressed as $A_B = -2.5 \log \left(\frac{1 - \exp(-\tau_B)}{\tau_B} \right)$, and in the range $10^8 - 10^{11} L_{B_\odot}$, using (4) with the central values, is well approximated by $A_B \approx 0.38 + 0.42 \log \left(\frac{L_B}{10^{10} L_{B_\odot}} \right) + 0.14 \left(\log \left(\frac{L_B}{10^{10} L_{B_\odot}} \right) \right)^2$. Now, applying this correction to the B-band luminosities given by our models, we are able to predict the B-band TF relation influenced by the extinction. Figure 7 shows that this relation in the range $\sim 10^9 - 10^{11} L_{B_\odot}$ is well approximated by a line with slope ~ 2.7 , i.e. the predicted TF relation now agrees with the observational estimates. Note that the luminosity dependence of the extinction does not only produce a change of slope, but also some nonlinearity, particularly at the bright end of Figure 7. A similar result was previously reported by Giovanelli et al. (1995), and this could be the reason for the different slopes given for the B-band TF relation by different authors. Recently, Kudrya et al. (1997) have presented the B-band TF relation for a large sample of galaxies; from their Figure 6 it is clearly seen how the slope of this relation tends to be steeper for the less luminous galaxies. Since the intrinsic dust absorption and the thickness of the dust layer with respect to a given stellar population tend to decrease with increasing wavelength, the change of slope in the TF relation will decrease as the passband tends to the H-band. Thus, the measured dependence of dust extinction on luminosity might explain part of the so called “color” TF relation rather well. In Figure 7 are also depicted the corrected TF relations corresponding to the two extreme cases of maximal and minimal optical depths, where $\tau_{B,*} = 1.1$ and $\beta = 0.7$, were used for the former, and $\tau_{B,*} = 0.5$ and $\beta = 0.3$ for the latter. The more realistic “sandwich” model (Disney, Davies, & Philipps 1989) was also considered. While β was not changed with respect to its fiducial value, $\tau_{B,*}$ and the ratio of the height scale of dust to young stars, ζ , were fixed to the values suggested by Bosselli & Gavazzi (1994) for the optically thin case in the H-band ($\tau_{B,*} = 1.33$ and $\zeta = 0.74$).

Wang & Heckman (1996) have pointed out that eq. (4) may be explained by the observed increase in the metallicity with the luminosity for which the dependence is considerable, $Z \propto L_B^\gamma$, with $\gamma \approx 0.3 - 0.5$ (see for references Roberts & Haynes 1994). The metallicity also influences the spectrophotometric evolutionary models. For example the models of Bressan, Chiosi, & Fagotto (1994) applied to single stellar populations with different initial metallicities show that at ~ 12 Gyr the differences in the V-K and B-V colors are ~ 0.88 mag and ~ 0.23 mag, respectively for a factor of 20 of variance in the metallicity. These models roughly agree with the observed color-magnitude relation of elliptical galaxies, and in accordance with Kodama & Arimoto (1997), this relation is consequence of a metallicity effect, instead of an age effect. We conclude that given the metallicity-mass relation observed in galaxies, extinction, and the spectrophotometric evolution, may be the basis for the color-magnitude and “color” TF relationships.

3.3. The fundamental physical factors of disk galaxies and the Hubble Sequence

The three main physical factors of the extended collapse scenario are the *total mass* M , the *MAH*, and the *angular momentum expressed through the spin parameter* λ ; these parameters, and

their correlations are related to the initial cosmological conditions. Analytical studies (Hoffman 1986, 1988; Heavens & Peacock 1988) suggest that λ is almost independent on the fluctuation peak height (related to the MAH) for CDM power spectra (but see Catelan & Theuns 1996). As a first approximation, here we consider that λ and the MAH are independent. We also assumed independence between λ and M (see §2.3). Concerning the dependence of MAH on M , for the CDM power spectra, the less massive galaxies show faster early collapses than do more massive galaxies (AFH). The correlation coefficients from a principal analysis of these 3 factors with the model galaxy (observable) properties are given in Table 2. The MAH was quantified through the γ parameter, where $\gamma = \frac{M_0 - M_0/2}{t(M_0) - t(M_0/2)}$. It is seen that the MAH, which drives the SF history, strongly influences B-V, and moderately influences the gas fraction. The range of B-V colors that the models span is mainly associated with the statistical dispersion in the MAHs. This dispersion is also reflected in the TF scatter, and as was shown above (see Figure 6) observations confirm a correlation between B-V and the maximum circular velocity for a given luminosity (mass). The λ parameter strongly influences the surface brightness, b/d ratio, and gas fraction, and slightly influences the color index. For a given M and MAH, λ determines the degree of concentration of disks. According to the SF mechanism used in our models, the stellar disks formed from more concentrated gaseous disks are typically “colder” than those emerged from less concentrated gaseous disks. Therefore, the stellar Toomre parameter is small for small λ 's. That is why the b/d ratio is closely related to λ . Mass strongly correlates with luminosity and the Holmberg radius, and slightly influences the b/d ratio and the surface brightness (both in the same direction as suggested by observations). As was pointed out in §3.2, B-V and μ_{B_o} are the two parameters from which the other intensive properties depend, i.e. the intensive properties of disk galaxies may be described in a biparametrical sequence, whose origin deals with two of the fundamental physical factors of galaxies, the MAH and λ , respectively. Most of these properties are almost invariant to the third factor, the mass (luminosity).

The morphological Hubble classification has been a useful guide to study the observational properties and correlations of galaxies. Nevertheless, most of the classification discriminators deal with morphological characteristics that probably are transient phenomena related to other more fundamental galactic characteristics. The main classification discriminators for spirals are the pitch angle and the strength of the spiral arms and bars. The problem of the origin and maintenance of arms in disk galaxies is however still not well understood. Within the framework of the density wave theory, feedback and amplification (overreflection) processes such as the “waser” mechanism (Mark 1976) were proposed in order to explain the self-excitation and persistence of spiral arms without any external driving, and in the so called modal approach (e.g., Bertin & Lin 1989a, 1989b and references therein) they are unified in one scheme which associates the spiral arm structure and the existence of bars with global modes of oscillation. Unfortunately, this and other approaches are not predictive in the sense that they do not provide us with a direct connection between the structural and dynamical properties of a given galactic model and the characteristics of its perturbed state (for example the arm pitch angle). Bertin et al. (1989a) have applied a global stability analysis to basic states defined by simple analytical expressions, and

found that the generated survey of models comprises the main morphological types, where three are the physical parameters which control the morphology: the gas fraction, the active disk mass with respect to the total mass, and the “temperature” of the stellar disk (see also Bertin & Lin 1996). It is interesting to note that if the b/d ratio is understood as a dynamical “thermometer” of the system, and μ_{B_0} as an indicator of the disk self-gravity, then according to the prediction of our models, galaxies fill only a planar region in the space of the three physical parameters which control the morphology.

Bertin & Romeo (1987), Bertin et al. (1989a,b) and other authors (see for references Combes 1993) coincide in pointing out that gas, dynamically speaking, is crucial for the excitation and maintenance of spiral structures. A purely stellar spiral would heat up quickly and disappear, producing a thickened, “hot” structure. *Accretion of gas, which is natural in the extended collapse scenario, will cool the stellar disk and give the conditions for instabilities.* Such a behavior has also been reported in N-body numerical simulations (Sellwood & Carlberg 1984). According to Bertin & Lin (1996), the gas fraction mainly determines the sequence of types a, b, and c, i.e. the pitch angle of arms. As is seen in Table 1, the gas fractions in our models correlates with the other secondary indicators of the HS which go across the a, b, and c sequence, such as μ_{B_0} , b/d, and B-V, showing that the origin of the Hubble morphological types is closely related to the galaxy formation and evolution processes of the extended collapse scenario.

Several authors have pointed out that for a given luminosity galaxies with larger maximum rotation velocities (the TF dispersion) are of earlier types than those with smaller velocities (Roberts 1978; Rubin et al. 1980; Rubin 1985; Giraud 1986, 1987; Krann-Korteweg, Cameron, & Tamman 1988; Giovanelli et al. 1997). The B-band TF relation, $L_{B_\odot} = A_{TF} V_{\max}^{m_B}$, predicted by the models has a dispersion that, to a first approximation, we express only through variations in the coefficient A_{TF} . As has been commented in § 3.2 (see also Figure 6), it turns out that the models present correlations between A_{TF} and some secondary Hubble type indicators: B-V, f_g , and b/d (see Table 1). Hence, within the framework of the extended collapse scenario the empirical correlation found between galactic type and rotation velocity for a given luminosity finds a natural explanation (see also § 3.2 and Figure 6).

4. Evolutionary models and intermediate redshift ($z \lesssim 1$) observations

With the advent of observational information for galaxies at different redshifts, an empirical picture of galaxy formation and evolution begins to be possible (e.g., Ellis 1998). In order to interpret the observational data of galaxies at intermediate and high redshifts, the theoretical models are crucial. The models presented here explain in principle the main characteristics of disk galaxies corresponding to the locally dominant galaxy population. Since these are evolutionary models, it is easy to predict how such a population will evolve.

The SF history (SFH) is a relevant evolutionary feature of galaxies. Within the framework

of our models the SFH is driven by the gas accretion rate (related to the MAH) and by the gas surface density (related to λ). The total mass aggregation rates at different redshifts for systems of $5 \times 10^{10} M_{\odot}$, $5 \times 10^{11} M_{\odot}$, and $5 \times 10^{12} M_{\odot}$ with the average MAHs are depicted in Figure 8(a) (SCDM, $\sigma_8 = 0.57$). In panel (b) the corresponding disk SF rates for $\lambda = 0.05$ are plotted; for the $5 \times 10^{11} M_{\odot}$ system, the SFHs corresponding to the very extended and early active MAHs, respectively ($\lambda = 0.05$), are also plotted. As it is seen the MAH clearly influences on the SFH. In Figure 8(c) one appreciates the influence on SFH of the disk surface density which depends on λ ; the dotted curves correspond to the SFHs of $5 \times 10^{11} M_{\odot}$ systems with the average MAH but with $\lambda = 0.035$ and $\lambda = 0.1$ (upper and lower curves, respectively). Also in this panel are plotted two extreme cases: a very extended MAH with $\lambda = 0.1$ (lower point-dashed curve), and an early, active MAH with $\lambda = 0.035$ (upper point-dashed curve). These are rare objects. The massive systems corresponding to early, active MAHs and low λ , might be of particular interest, because these are luminous, very active SF objects at early times which could correspond to galaxies seen at very high redshifts (Avila-Reese 1998; see also Baugh et al. 1997).

According to Figure 8(b), the maximum in the SF activity of the models which corresponds to a normal disk galaxy population, is attained at $z \sim 1.5 - 2.5$; after this, for almost all the cases, the SF rate moderately decreases until the present epoch by a factor $\sim 2 - 4$. Recently, Lilly et al. (1997) have studied the evolution of a large disk galaxy population using a combination of the observational data from the CNRS redshift survey and the Hubble Deep Field; they estimated a moderate decrease in the SF rate, a factor 2.5-3.5 between $z \approx 0.7$ and $z \approx 0.0$ (for the models, in this case, the factor is ~ 2). Deep field studies, where no population selection was made, show that the global (cosmic) SFH per unit of volume increases from $z \approx 0$ to $z \approx 0.7$ by a factor ~ 6 and by more than a factor of 10 up to the maximum which is attained at $z \approx 1.5 - 2.0$ (e.g., Madau, Pozzetti, & Dickinson 1997, and the references therein). If our models actually describe the evolution of the normal disk galaxy population which dominates the luminosity and SF rate today, then the high global SF rate (and luminosity) observationally estimated at $z \approx 1 - 2$, can not be produced by this population.

In the extended collapse scenario disk galaxies form inside-out by a continuous process of mass aggregation and are not expected to undergo abrupt evolutionary changes in their structural and luminosity characteristics. The evolution of h_d , μ_{B_o} , and the bulge-to-total mass (luminosity) ratio for models corresponding to $5 \times 10^{10} M_{\odot}$, $5 \times 10^{11} M_{\odot}$, and $5 \times 10^{12} M_{\odot}$ systems with the average MAHs and $\lambda = 0.05$ are depicted in Figure 9(a), 9(b), and 10, respectively. Lilly et al. (1997), for the galaxy population they studied, estimated a maximum decrease in the scale radius of 25% from $z \approx 0$ to $z \approx 1$ (the circle with a cross in panel (a)). At the same time, from $z \approx 0$ to $z \approx 0.7$, they estimated an increase in the central surface brightness (B-band) corresponding to ~ 0.9 mag/arcsec² (the circle with a cross in panel (b)). The evolution of the bulge-to-total ratio is less clear. If we take the average ratios given in Lilly et al. (1997) at $\langle z \rangle = 0.375$ and $\langle z \rangle = 0.625$ we obtain a slope, that after normalizing to $z = 0$, corresponds to the segment plotted in Figure 10. An interesting prediction of our “secular” recipe for bulge formation is that the less

massive systems form their bulges later than the more massive systems.

The evolution of the B-band TF relation can be related to (i) the structural evolution of the galactic system and (ii) to the B-band luminosity evolution. The models (average MAH and $\lambda = 0.05$) show that the “structural” TF relation, $M_s = AV_{\max}^m$ (or equivalently the H- or I-band TF relation), has minimal slope changes with z , while the zero-point A decreases between $z = 0$ and $z = 0.7$ by a factor of 2 (0.75 mag) and between $z = 0$ and $z = 1.7$ by a factor of 3 (1.20 mag). The luminosity with $z \rightarrow 1.5 - 2.5$ increases by a factor of 2 – 3 for most of the models. Regarding the model B-band TF relation, its slope also remains approximately the same in the past, while the zero point increases with z , but not significantly (~ 0.1 mag and ~ 0.45 mag for the mentioned redshift intervals). The B-band TF relation remains almost the same with z due to the compensation of 2 effects: the structural evolution of the system and the luminous evolution of the disk. Vogt et al. (1997), from a deep field study (up to $z \approx 0.7$), have concluded that the slope of the B-band TF relation does not change, while the zero-point could increase no more than 0.4 mag.

5. Conclusions

We have modeled the formation and evolution of disk galaxies within the framework of the extended collapse scenario, which is based on the inflationary CDM models. The gas disks in centrifugal equilibrium were built-up under the assumption of detailed angular momentum conservation into spherical virializing dark matter halos whose MAHs were calculated from the initial cosmological conditions. The disk SF is produced by global gravitational instabilities and is self-regulated by an energetic balance of the turbulent gas. The bulges are formed by secular evolution of the stellar disk based on gravitational instabilities. The main predictions of the models are:

- 1). The disks present exponential surface brightness profiles and negative radial B-V gradients. The scale lengths and central surface brightnesses are in agreement with the observations, including the LSB galaxies.
- 2). The rotation curves are nearly flat up to the Holmberg radius. Contrary to observational estimations, the rotation curve decompositions show dominion of dark matter down to the galaxy central regions. A constant density core in the dark halo solves this problem.
- 3). The intensive properties and their correlations (particularly those which go across the HS) of the models corresponding to the local ($z \approx 0$) population of disk galaxies, including the LSB galaxies, are determined by the combination of three fundamental physical factors and their statistical distributions, related to the initial cosmological conditions. These three factors are the mass, the MAH, and the primordial angular momentum expressed through the spin parameter λ .
- 4). The intensive properties of the models can be described in a biparametrical sequence,

where the parameters may be the color index B-V and the central surface brightness μ_{B_o} . Each one of these parameters is determined mainly by the MAH and λ , respectively. The third fundamental physical factor, the mass, exerts no practical influence the intensive properties. We have shown that the empirical luminosity (mass)-color relation (or equivalently the color TF relation) can be explained by the effects of the metallicity and the extinction. observed dependence of extinction on luminosity (mass). These effects also contribute to decrease the slope of the B-band TF relation.

5). The SF rates of models with the average MAHs and $\lambda = 0.05$ grow by factors of 2.5-4.0 up to $z \sim 1.5 - 2.5$ with respect to the SF rates at $z = 0$. After this maximum, the SF rates slowly decrease with z . The SFHs of systems with early, active MAH and/or low λ 's show high SF rates at high redshifts ($z > 3$), while the systems with extended MAHs and/or high λ 's present small SF rates which slowly increase until the present epoch.

6). The structural properties of the models do not change abruptly. Between $z = 0$ and $z \approx 1$ the disk scale radii in average decrease a factor ~ 1.3 and the central surface brightnesses increase ~ 1 mag/arcsec². The bulge-to-total luminosity ratio also decreases with z and decreases more severely for the low mass systems. The slopes of the “structural” and B-band TF relations do not change with z . In the case of the “structural” TF relation, the zero-point decreases (0.75 mag for $z = 0.7$ with respect to $z = 0$), while for the B-band TF relation the zero-point slightly increases (0.1 mag at $z = 0.7$ with respect to $z = 0$).

The exploratory models presented in this work show that the main observational characteristics and correlations of disk galaxies can be well understood in the context of the extended collapse scenario, suggesting a direct connection between the conditions prevailing in the early universe and the properties of galaxies today. A serious shortcoming of galaxies emerging from Gaussian CDM cosmological models is the gravitational dominion of DM over baryon matter. The remedy to this problem is the introduction of a core in the DM halo. Fortunately, the intensive galaxy properties and their correlations are not significantly sensitive to the existence or non-existence of such a core, in such a way that all the results presented here are also true for galaxies with a core in their DM halos. The main limitations of our approach are connected to the facts that (i) the influence of the environment on galaxy formation and evolution was not taken into account, (ii) detailed angular momentum conservation for the baryon gas collapse was assumed, and (iii) the mass aggregation was treated only as gas accretion neglecting the possibility of mergers of stellar systems. In future we shall address ways of overcoming these limitations with the aim to improve the model predictions and to explain galactic properties and distributions related to environment.

V.A.-R. acknowledges the support of a fellowship from the project UNAM-DGAPA IN-105894 and support from the program “Becas Cuauhtémoc” of CONACyT. C.F and V.A.-R. would like to acknowledge to Antonio Garcés for his computing assistance.

- Avila-Reese, V. 1998, Ph.D. Thesis, U.N.A.M (in spanish).
- Avila-Reese, V., Firmani, C., & Hernández, X. 1997, ApJ, accepted (astro-ph/9710201) (AFH)
- Baugh, C.M., Cole, S., & Frenk, C.S. 1996, MNRAS, 283, 1361
- Baugh, C.M., Cole, S., & Frenk, C.S., & Lacey, C. 1997, submitted to ApJ, (astro-ph/9703111)
- Begeman, K. 1987, Ph.D. Thesis, University of Groningen
- Bertin, G., & Lin, C.C. 1996, “Spiral Structure in Galaxies. A Density Wave Theory” (The MIT Press)
- Bertin, G., & Romeo, A.B. 1988, A&A, 195, 105
- Bertin, G., Lin, C.C., Lowe, S.A., & Thurstans, R.P. 1989a, ApJ, 338, 78
- . 1989b, ApJ, 338, 104
- Boselli, A., & Gavazzi, G. 1994, A&A, 283, 12
- Bressan, A., Chiosi, C., & Fagotto, F. 1994, ApJS, 94, 63
- Burkert, A. 1995, ApJ, 447, L25
- Bruzual, G.A., & Charlot, S. 1993, ApJ, 405, 538
- Cardelli, J.A., Clayton, G.C., & Mathis, J.S. 1989, ApJ, 345, 245
- Carignan, C., & Freeman, K.C. 1985, ApJ, 160, 811
- Carlberg, R.G. 1985, in “The Milky Way Galaxy”, proceedings of the 106th Symposium (Dordrecht, D.Reidel Publishing Co.), 615
- Catelan, P., & Theuns, T. 1996, MNRAS, 282, 436
- Charlot, S., Worthey, G., & Bressan A. 1996, ApJ, 457, 625
- Cole, S., Aragon-Salamanca, A., Frenk, C.S., Navarro, J., & Zepf, S. 1994, MNRAS, 271, 781
- Combes, F. 1993, in “The Formation and Evolution of Galaxies”, eds. Muñoz-Tuñón & F. Sánchez (Cambridge Univ. Press), p. 317
- Courteau, S., de Jong, R.S., & Broeils, A.H. 1997, ApJ, 457, L73
- de Jong, R.S. 1995, Ph.D. Thesis, University of Groningen
- . 1996a, A&A, 313, 45
- . 1996b, A&ASS, 118, 557

- de Vaucouleurs, G., et al. 1991, Third Reference Catalogue of Bright Galaxies (Springer, Berlin Heidelberg New York)
- Dekel, A., & Silk, J. 1986, ApJ, 303, 39
- Disney, M.J., Davies, J., & Philipps, S. 1989, MNRAS, 205, 1253
- Ellis, R.S 1998, in “Cosmological Parameters & Evolution of the Universe”, ed. K.Sato, IAU Symposium 183, in press
- Gallagher, J.S., Hunter, D.A., & Tutukov, A.V. 1984, ApJ, 284, 544
- Firmani, C., & Tutukov, A.V. 1992, A&A, 264, 37
- . 1994, A&A, 288, 713
- Firmani, C., Hernández, X., & Gallagher 1996, A&A, 308, 403
- Flores, R.A., Primack, J.R., Blumenthal, G.R., & Faber, S.M. 1993, ApJ, 412, 443
- Fritze-v.Alvensleben, U., & Gerhard, O.E. 1994, A&A, 285, 751
- Gavazzi, G. 1993, ApJ, 419, 469
- Giovanelli, R., Haynes, M.P., Herter, T.H., Vogt, N.P., da Costa, L.N., Freudling, W., Salzer, J.J., & Wegner, G. 1997, AJ, 113, 53
- Giovanelli, R., Haynes, M., Salzer, J.J., Wegner, G., Da Costa, L.N., Freudling, W. 1995, AJ, 110, 1059
- Giraud, E. 1986, ApJ, 309, 512
- . 1987, A&A, 174, 23
- Gunn, J.E. 1981, in “Astrophysical Cosmology”, M.S. Longair, Coyne G.V., & H.A. Brück, eds. (Pontificia Academia Scientarium:Citta del Vaticano), p.191
- . 1987, in “The Galaxy”, G. Gilmore & B. Carswell, eds. (Reidel Publishing Company), p.413
- Heavens, A., & Peacock, J. 1988, MNRAS, 232, 339
- Hoffman, Y. 1986, ApJ, 301, 65
- . 1988, ApJ, 329,8
- Kauffmann, G. 1995, MNRAS, 274, 161
- . 1996, MNRAS, 281, 475

- Kauffmann, G., White, S.D.M., & Guiderdoni, B. 1993, MNRAS, 264, 201
- Kennicutt, R.C. 1983, ApJ, 272, 5
- . 1989, ApJ, 344, 6854
- Kennicutt, R.C., Tamblyn, P., & Congdon, C.W. 1994, ApJ, 435, 22
- Kodama, T., & Arimoto, N. 1997, A&A, 320, 41
- Kraan-Korteweg, R.C., Cameron, L.M., & Tammann, G.A. 1988, ApJ, 331, 620
- Kudrya, Yu.N., Karachentseva, V.E., Karachentsev, I.D, & Parnovsky, S.L. 1997, Pis'ma v Astronomicheskii Jurnal, 23, 730 (in Russian)
- Lacey, C.G., Guiderdoni, B., Rocca-Volmerange, & B.Silk, J. 1993, ApJ, 402, 15
- Larson, R.B. 1992, in “Star Formation in Stellar Systems”, G.Tenorio-Tagle, M.Prieto, & F.Sánchez, eds. (Cambridge University Press), p.125
- Larson, R.B., & Tinsley, B. M. 1978, ApJ, 219, 46
- Larson, R.B., & Tinsley, B. M., & Caldwell, C.N. 1980, ApJ, 237, 692
- Lilly, S.J. et al. 1997, preprint (astro-ph/9712061)
- Madau, P., Pozzetti, L., & Dickinson, M. 1997, preprint (astro-ph/9708220)
- Mark, J.W.-K. 1976, ApJ, 205, 363
- McGaugh, S.S., de Blok, W.J.G. 1997, ApJ, 481, 689
- Norman, C.A., Sellwood, J.A., & Hassan, H. 1996, ApJ, 462, 114
- Nulsen, P.E.J., & Fabian, A.C. 1995, MNRAS, 277, 561
- Peletier, R., & Balcells, M. 1996, AJ, 111, 2238
- Persic, P., Salucci, M., & Stel, F. 1996, MNRAS, 281, 27
- Renzini, A. 1994, in “Galaxy Formation”, J.Silk & N. Vittorio, eds. (Elsevier Science Publishers B.V., The Netherlands), p.303
- Rees, M.J., & Ostriker, J.P. 1977, MNRAS, 179, 541
- Roberts, M.S. 1978, AJ, 83, 1026
- Roberts, M.S., & Haynes, M.P. 1994, ARA&A, 32, 115
- Sandage, A. 1961, The Hubble Atlas of Galaxies (Carnegie Inst. of Washington, Washington DC)

- Rubin, V.C., Burstein, D., Ford, W.K., & Thonnard, N. 1980, *ApJ*, 238, 471
- . 1985, *ApJ*, 289, 81
- Ryden, B.S., & Gunn, J.E. 1987, *ApJ*, 318, 15
- Sellwood, J.A., & Carlberg R.G. 1984, *ApJ*, 282, 61
- Silk, J. 1977, *ApJ*, 211, 638
- Simien, F., & de Vaucouleurs, G. 1986, *ApJ*, 302, 564
- Skillman, E.D. 1987, in “Star Formation in Galaxies”, C.J. Lonsdale, ed. (NASA Conference Publication N0. 2466, Washington), p.263
- Strauss, M.A., & Willick, J.A. 1995, *Phys. Rep.*, 261, 271
- Tinsley, B. 1980, *Fundamental Cosmic Phys.*, 5, 287
- Toomre, A. 1964, *ApJ*, 139, 1217
- Tóth, G., & Ostriker, J.P. 1992, *ApJ*, 389, 5
- Tully, R.B. 1988, *Nearby Galaxies Catalog* (Cambridge, U.P.)
- Tully, B., Mould, J., & Aaranson, M. 1982, *ApJ*, 257, 527
- Vogt, N. et al. 1997, *ApJ*, 479, L121
- Vishnavatan, N. 1981, *A&A*, 100, L20
- Wang, B., & Heckman, T.M. 1996, *ApJ*, 457, 645
- White, S.D.M. 1994, preprint MPA 831
- White, S.D.M., & Frenk, C.S. 1991, *ApJ*, 379, 52
- White, S.D.M., & Rees, M.J. 1978, *MNRAS*, 183, 341
- White, S.D.M., Efastathiou, G., & Frenk, C.S. 1993, *MNRAS*, 262, 1023
- Wyse, R. 1982, *MNRAS*, 199, 1P
- Wyse, R.F.G., Gilmore, G., & Franx, M. 1997, *ARA&A*, 35, 637

Table 1. Correlation matrix of the global properties

	B-V	f_g	b/d	M_B	V_m	$\log h_d$	A_{TF}
μ_{B_0}	-0.07	0.84	-0.93	0.55	-0.65	0.29	0.33
B-V	...	-0.56	0.18	0.22	-0.05	-0.29	-0.82
f_g	-0.87	0.27	-0.45	-0.01	0.68
b/d	-0.38	0.54	0.10	-0.51
M_B	-0.94	-0.95	-0.20
V_m	0.84	-0.04
$\log h_d$	0.34

Table 2. Correlation matrix of the global properties and the fundamental parameters

	μ_{B_0}	B-V	f_g	b/d	M_B	V_m	$\log h_d$	A_{TF}
$\log M_0^{(a)}$	-0.44	-0.24	-0.17	0.27	-0.9	0.92	0.98	0.25
$\gamma^{(b)}$	0.01	-0.95	0.48	-0.12	-0.24	0.05	0.29	0.82
$\lambda^{(c)}$	0.86	-0.07	0.81	-0.88	0.13	-0.23	0.51	0.34

^(a)present-day mass

$$\text{(b)} \gamma = \frac{M_0 - M_{0/2}}{t(M_0) - t(M_{0/2})}$$

^(c)spin parameter

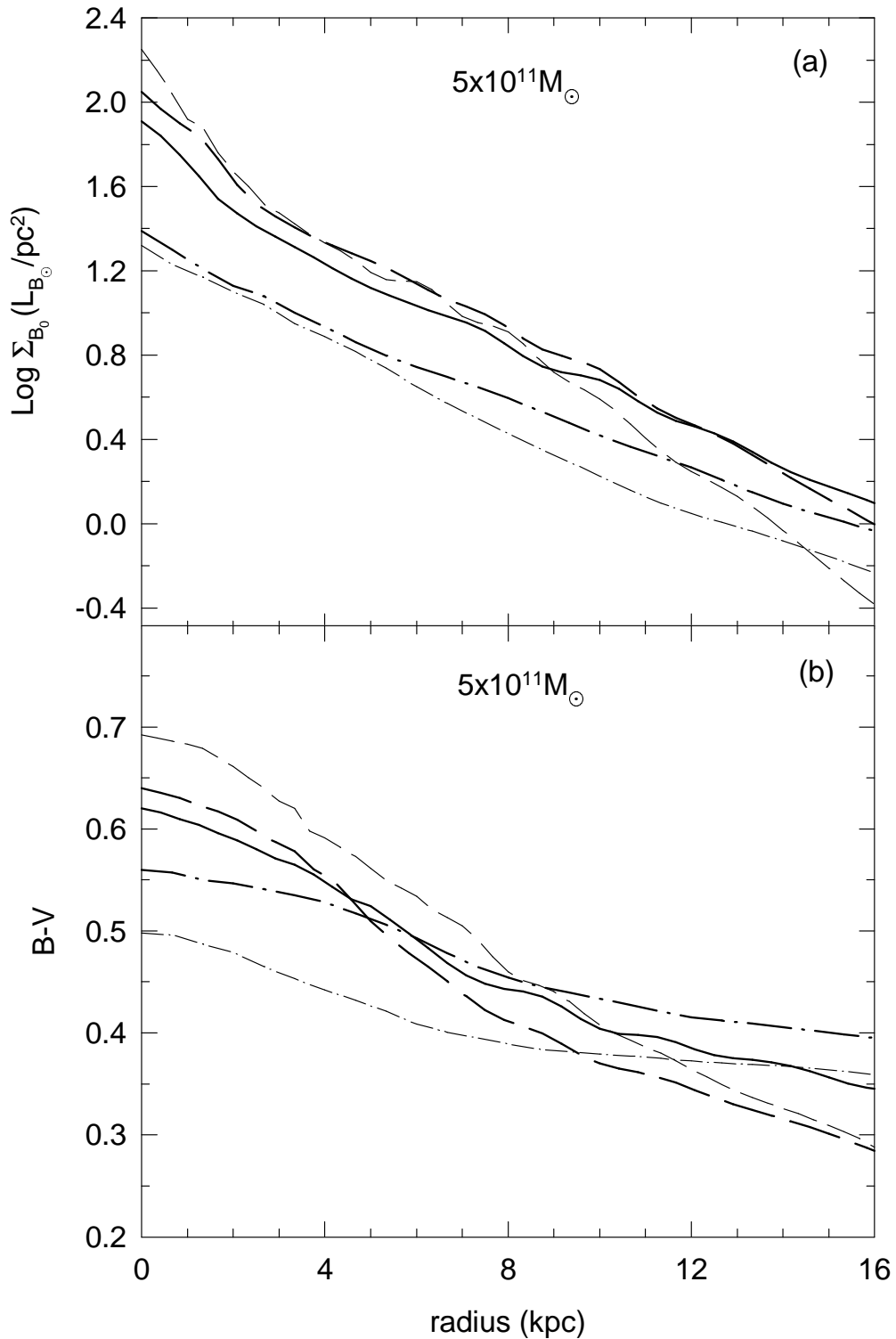


Fig. 1.— The B-surface brightness (a) and the B-V color index (b) profiles of a $5 \times 10^{11} M_{\odot}$ galaxy. The average MAH cases for the spin parameters $\lambda = 0.035$ (dashed line), $\lambda = 0.050$ (solid line), and $\lambda = 0.100$ (point-dashed line) are represented with the thick lines. For the early active MAH only the model with $\lambda = 0.035$ (thin dashed line) is plotted, while for the extended MAH, only the $\lambda = 0.100$ case (thin point-dashed line) is shown. All the models were calculated for a $\sigma_8 = 0.57$ SCDM model.

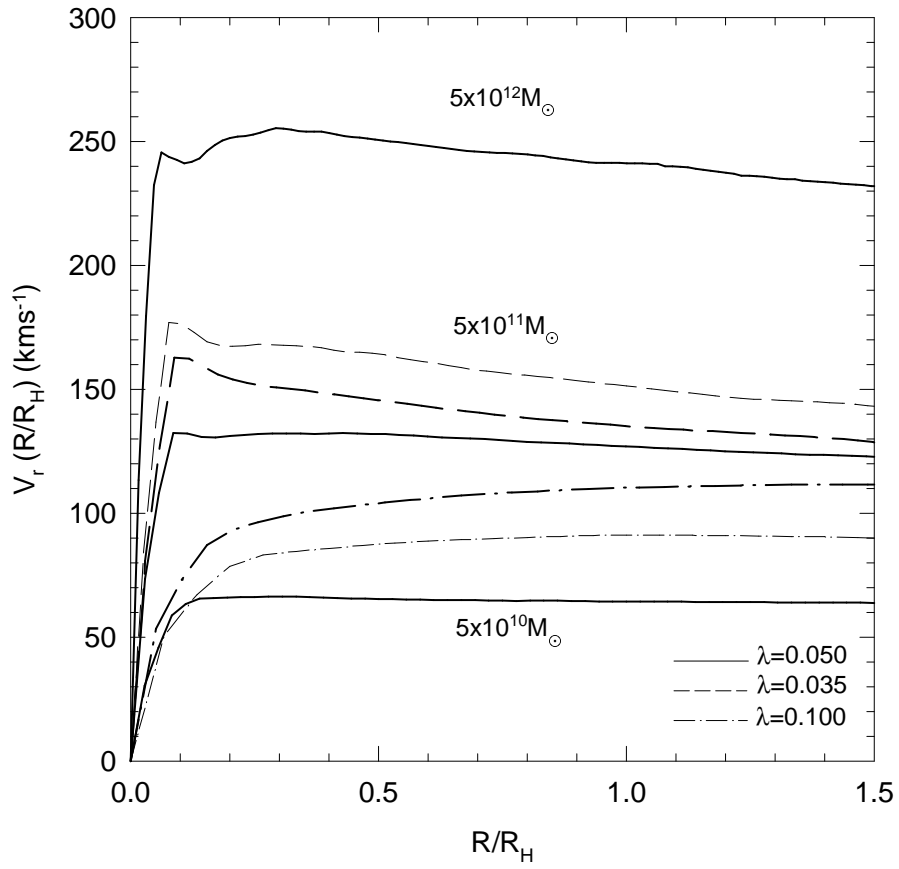


Fig. 2.— Rotation curves for the same models of Figure 1 ($5 \times 10^{11} M_\odot$), and for a $5 \times 10^{10} M_\odot$ (bottom curve) and $5 \times 10^{12} M_\odot$ (top curve) galaxy corresponding only to the average MAH, $\lambda = 0.050$. Radii were scaled to the optical (Holmberg) radii of each model.

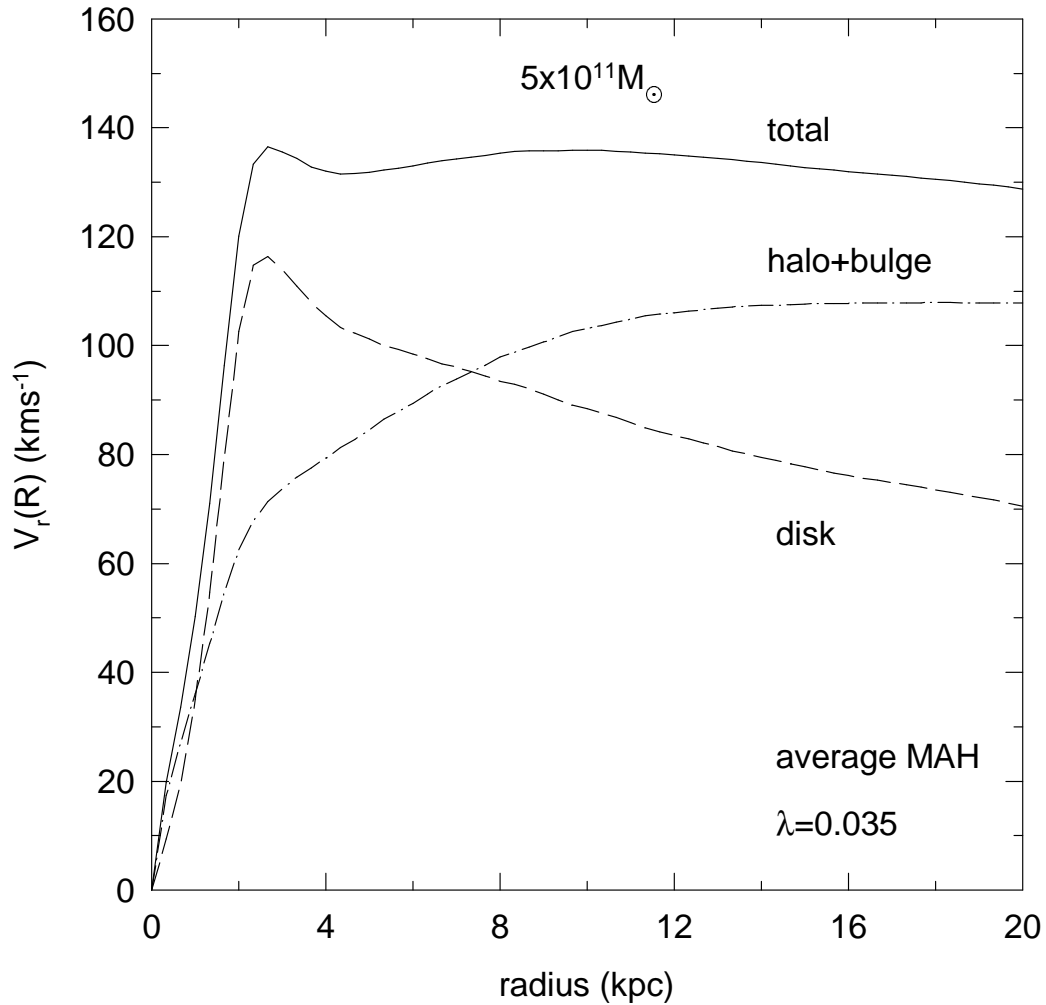


Fig. 3.— Rotation curve decomposition of a $5 \times 10^{11} M_{\odot}$ galaxy (average MAH and $\lambda = 0.05$), in the DM halo of which an artificial near constant-density core was introduced. The size of the core was calculated in accordance with the observational data for the dwarf galaxies (see text). Compare this Figure with Figure 4 of AFH where the rotation curve decomposition of a galaxy without a core is presented.

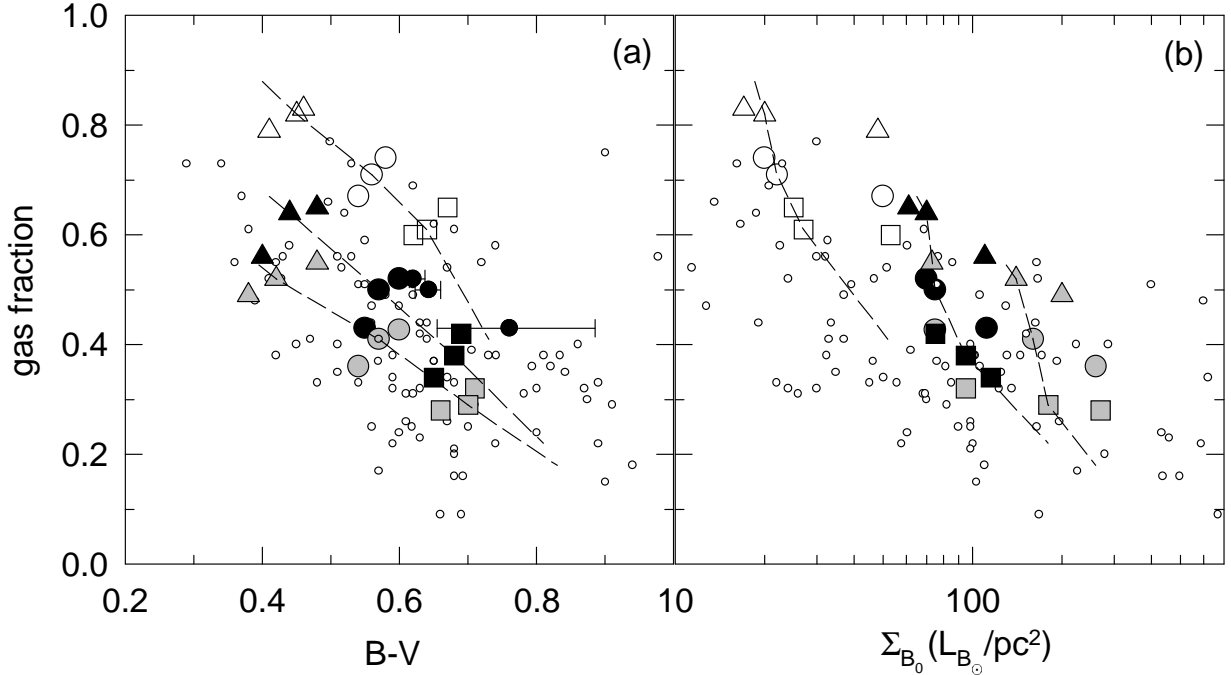


Fig. 4.— The gas fraction f_g vs. the integral B-V color index (a), and vs. the central B-surface brightness μ_{B_0} (b) for models and observations. The gray, black, and white filled symbols, correspond to models with $\lambda = 0.035$, $\lambda = 0.050$, and $\lambda = 0.100$ respectively. Squares are for the early active MAH, circles for the average MAH, and triangles for the extended MAH. Three masses (dark+baryon), $5 \times 10^{10} M_{\odot}$, $5 \times 10^{11} M_{\odot}$, and $5 \times 10^{12} M_{\odot}$ are considered (the larger the mass, the smaller is the gas fraction). The dashed lines connect the models of constant mass for $5 \times 10^{11} M_{\odot}$, and extend the statistical range of MAHs to 94% (symbols consider only 80% of the MAHs). The three small black filled circles are the same models corresponding to the big black filled circles but reddened according to the dust absorption-luminosity dependence given in Wang & Heckman (1996) (see text). The error bars correspond to the range of values which fit observational data. Small empty circles are the observational data collected by McGaugh & de Blok (1996) and corrected for inclination extinction. LSB galaxies are included.

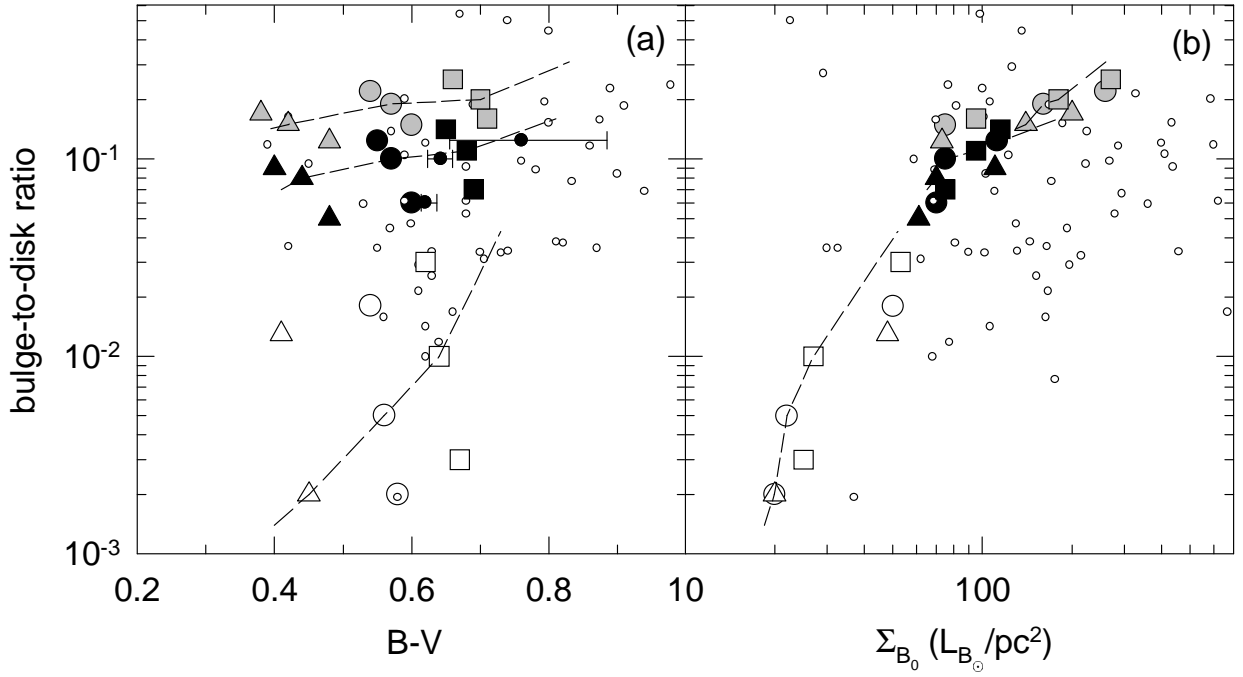


Fig. 5.— The bulge-to disk ratio vs the integral B-V color index (a), and the central B-surface brightness μ_{B_0} (b) for models and observations. The same symbol and line codes of Figure 4 are used. The bulge-to-disk ratios were taken from the K-band two-dimensional decompositions carried out by de Jong (1996b). LSB galaxies and a few normal galaxies shown in Figure 4 are absent in this Figure.

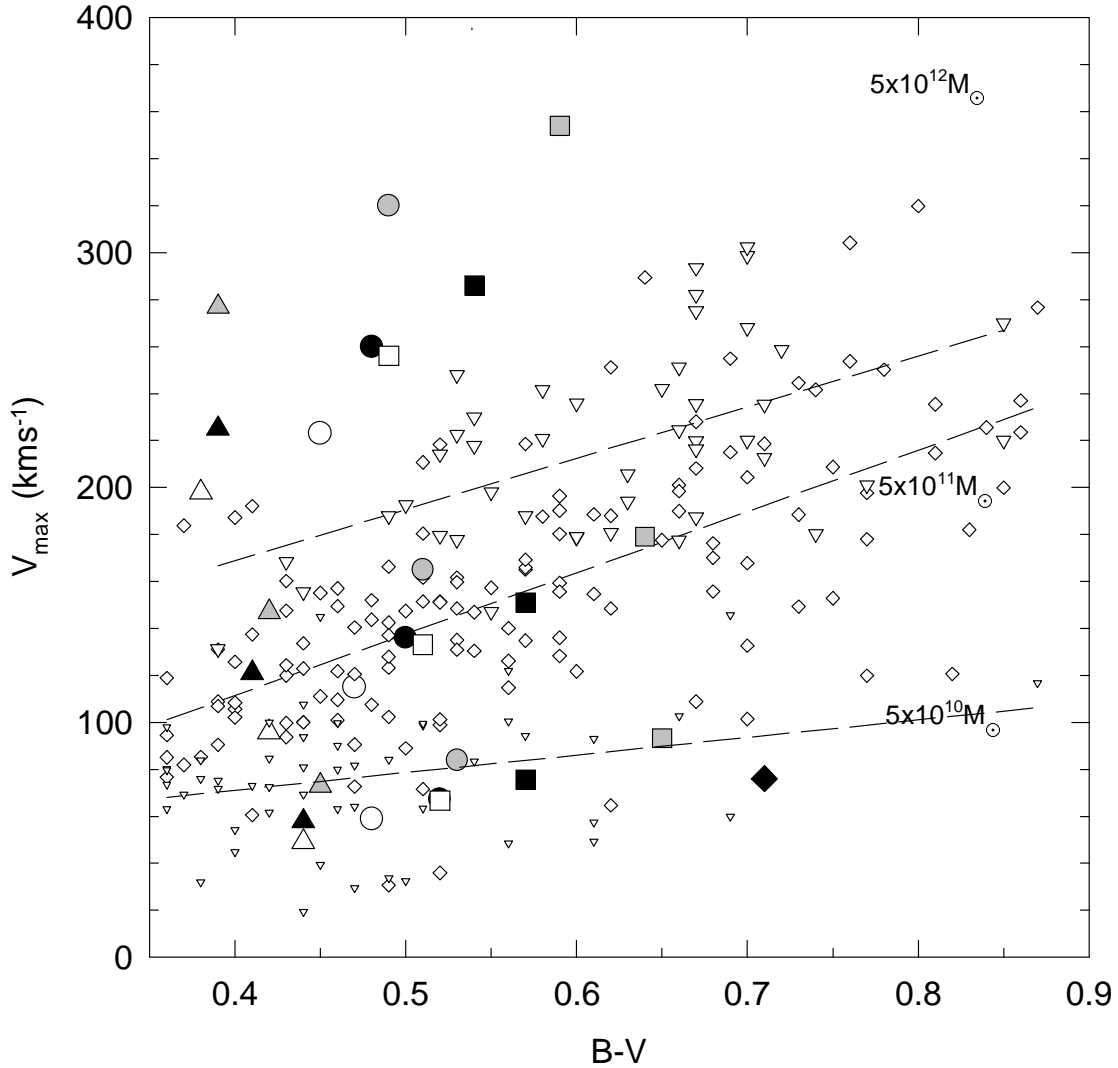


Fig. 6.— The maximum rotation velocity vs. B-V for models and observations. The same symbol codes of Figure 4 are used. The observational data (small symbols) were taken from a cross of the RC3 and the Tully (1988) catalogs (see text). The small triangles, diamonds, and inverse triangles correspond to galaxies with luminosities in B band within the $10^8 - 3 \times 10^9 L_{B_{\odot}}$, $3 \times 10^9 - 3 \times 10^{10} L_{B_{\odot}}$, and $3 \times 10^{10} - 2 \times 10^{11} L_{B_{\odot}}$ ranges, respectively. The dashed lines are linear regressions to the observational data corresponding to these ranges. Note how the maximum velocity of models and observations for a given mass (or range of luminosities) correlates with the B-V color.

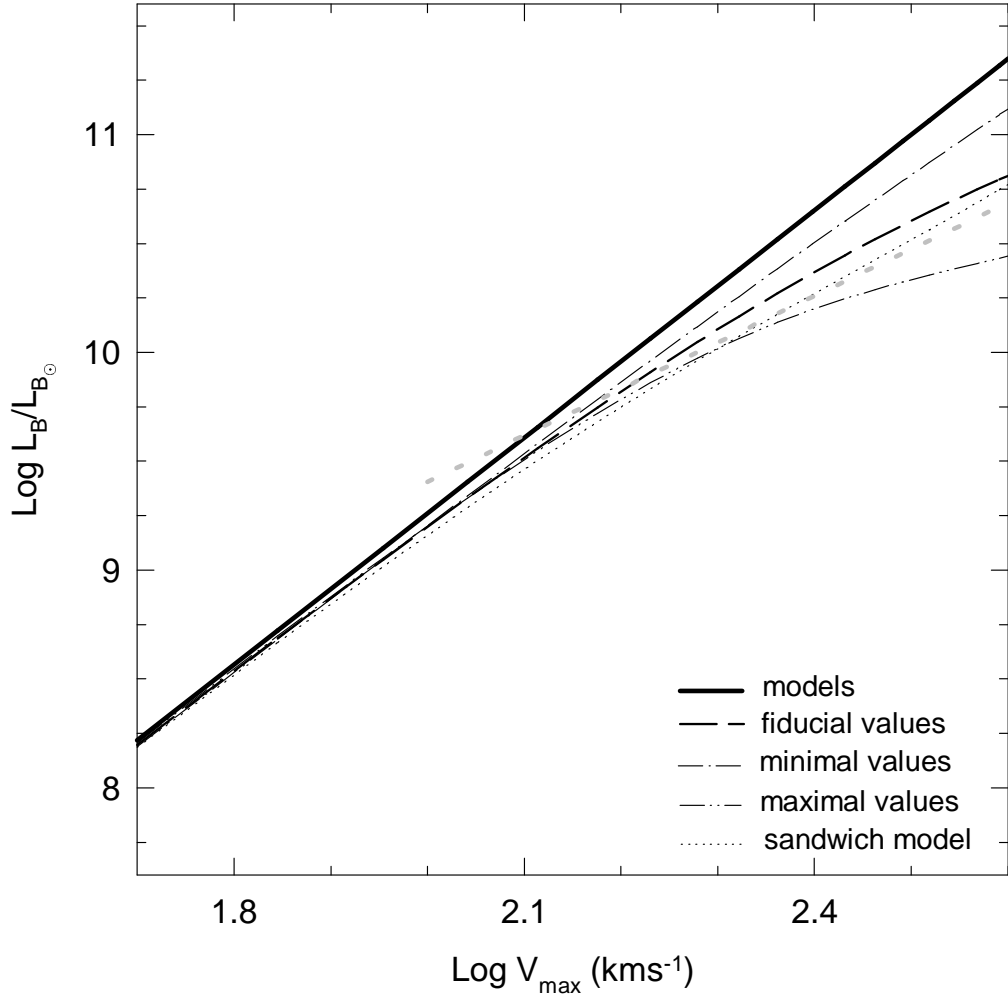


Fig. 7.— The predicted B-band TF relation for the $\sigma_8 = 0.57$ SCDM model (thick solid line). The slope of this relation is 3.5. The other lines show how the intrinsic TF relation transform if the B-luminosities are diminished by dust absorption according to the observational dependence of optical depth of dust on luminosity given in Wang & Heckman (1996). While the dashed line corresponds to the fiducial optical depth, the point-dashed and two point-dashed lines are for two extreme cases of maximal and minimal optical depths (see text). The point line was obtained using a sandwich model with a ratio of height scale of dust to young stars of 0.74 (see text for references). In the range $10^9 - 10^{11} L_{B_\odot}$ the dashed line is well approximated by a line with slope ~ 2.7 . The dotted gray curve is the linear regression to the empirical correlation between the absolute magnitude in B and the H21 linewidth, W_{50}^{corr} , given in Kudrya et al. (1997). We have assumed $W_{50}^{corr} = 2 \times V_{\max}$. We have truncated the regression at $V_{\max} = 100$ km/s because it does not provide a good approximation for lower velocities (see Figure 6 of Kudrya et al. 1997).

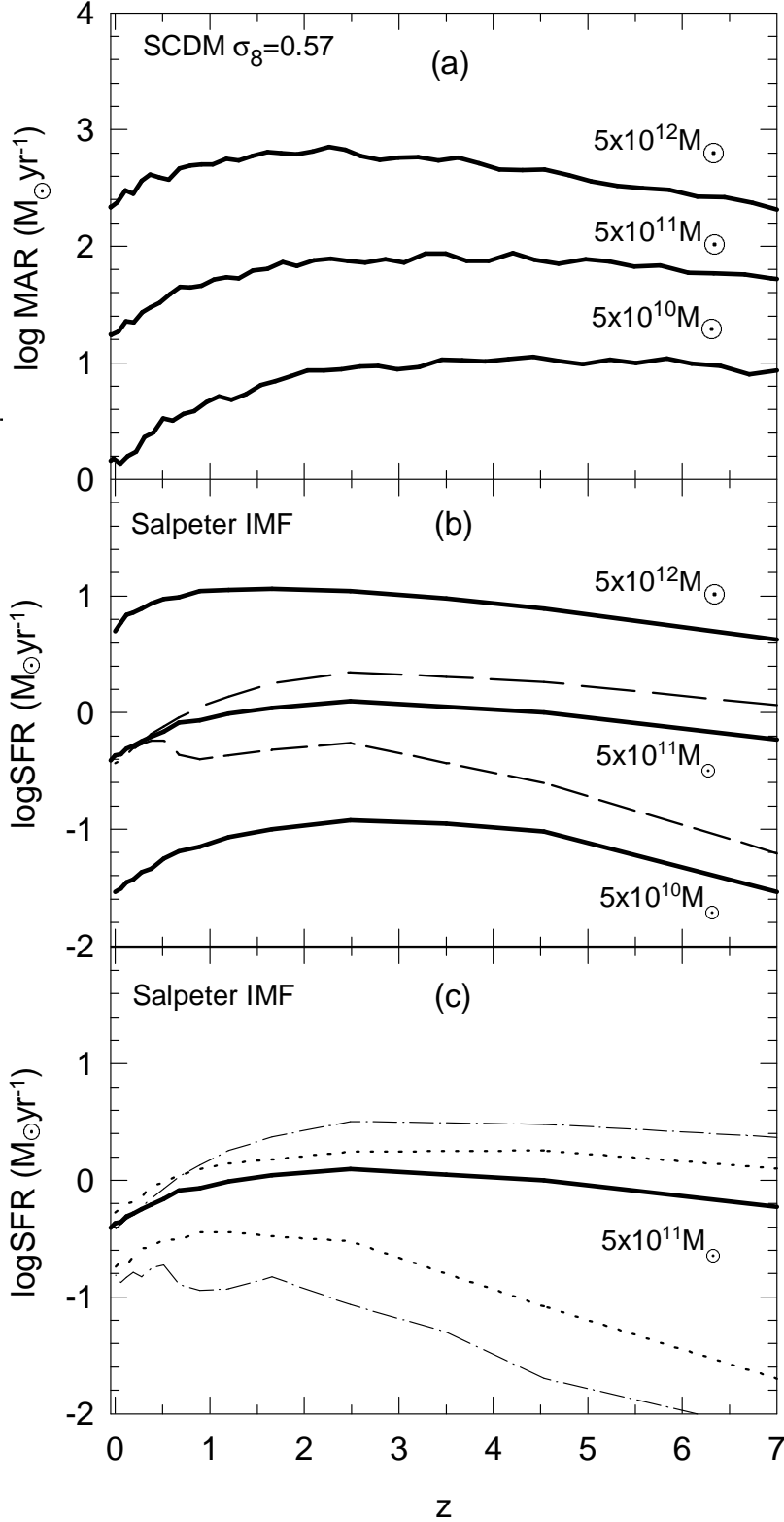


Fig. 8.— In panels (a) and (b) are plotted the total mass aggregation rates (MAR), and the SF rates vs. the redshift for systems of $5 \times 10^{10} M_\odot$, $5 \times 10^{11} M_\odot$, and $5 \times 10^{12} M_\odot$ with the average MAHs and $\lambda = 0.05$, respectively. In panel (b), for systems of $5 \times 10^{11} M_\odot$, are also depicted the SFHs corresponding to the early active MAH (upper dashed curve), and to the very extended MAH (lower dashed curve). The SFHs for for systems of $5 \times 10^{11} M_\odot$, with the average MAHs, but with $\lambda = 0.035$ (upper dotted curve), and with $\lambda = 0.1$ (lower dotted curve) are plotted in panel (c). Here the upper and lower point-dashed curves correspond to the extreme cases of an early active MAH with $\lambda = 0.035$, and a very extended MAH with $\lambda = 0.1$, respectively.

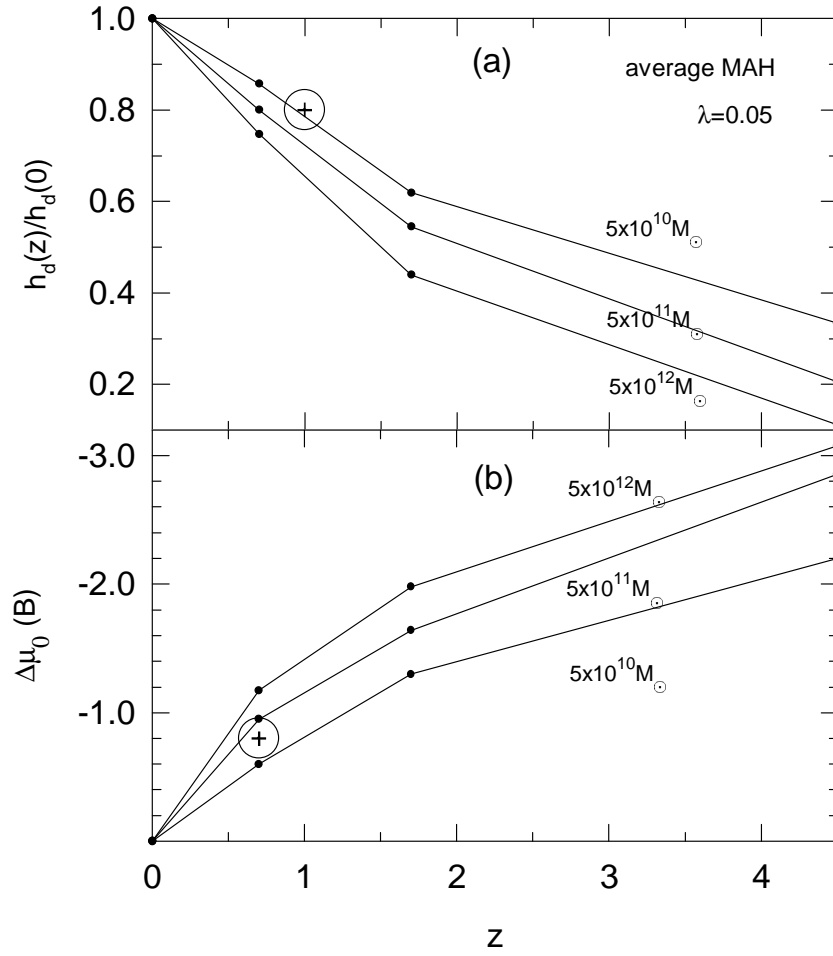


Fig. 9.— Evolution with z of the disk scale radius scaled to the radius at $z = 0$ (a), and of the difference in $\text{mag}/\text{arcsec}^2$ of the central surface B-brightness with respect to its value at $z = 0$ (b), for models corresponding to systems of $5 \times 10^{10} M_\odot$, $5 \times 10^{11} M_\odot$, and $5 \times 10^{12} M_\odot$ with the average MAHs and $\lambda = 0.05$. The circles with a cross indicate the corresponding estimations obtained from deep field observational studies of a bright spiral galaxy population (Lilly et al. 1997).

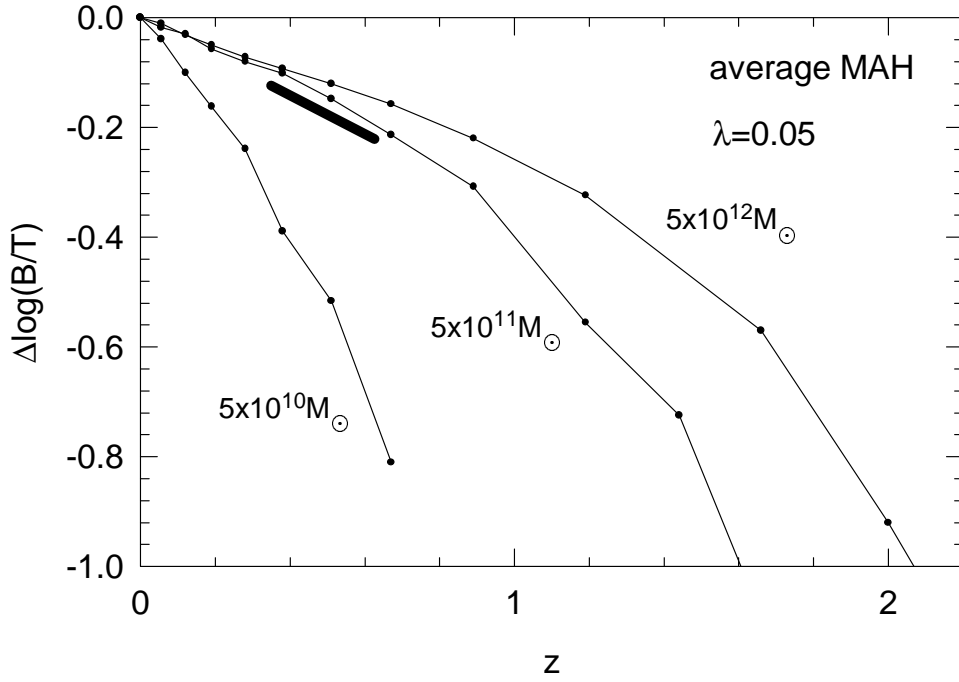


Fig. 10.— Evolution of the bulge-to-total luminosity ratio for the same models of figure 9. $\Delta \log(b/t) \equiv \log(b/t)(z) - \log(b/t)(0)$. The thick segment corresponds to the slope inferred from the observational data presented in Lilly et al. 1997 (see text).